Oxygen diffusion coefficient in the γ phase of a TiAl GE alloy determined by SIMS

Camille Thenot, Daniel Monceau, Damien Connétable, Pierre Sallot, Marie-Amandine Pinault-Thaury, Jean-Philippe Monchoux

Oxygen diffusion coefficient in the γ phase of a TiAl GE alloy determined by SIMS

Camille Thenot[1,2], Daniel Monceau[2], Damien Connétable[2], Pierre Sallot[3], Marie-Amandine Pinault-Thaury[4], Jean-Philippe Monchoux.[1*]

[1]CEMES, CNRS, Université de Toulouse, 31055, France.

[2]CIRIMAT, Université de Toulouse, CNRS, ENSIACET, 4 allée Emile Monso, 31030 Toulouse, France

[3]Safran Tech, Materials and Processes, Rue des Jeunes Bois, Châteaufort, 78114 Magny-Les-Hameaux, France

[4]Université Paris-Saclay, UVSQ, CNRS, GEMaC, 78000 Versailles, France

*Corresponding author. Email: monchoux@cemes.fr

Abstract:

First reliable experimental oxygen diffusion coefficient data have been obtained in a $Ti_{48.3}Al_{47.7}Cr_{1.9}Nb_{2.1}$ near-γ GE alloy through secondary ion mass spectrometry (SIMS) depth profiling measurements of ^{18}O isotopes between 500°C and 700°C. The following expression of diffusion coefficient D has thus been derived: $D\left(\mathrm{m^2/s}\right) = 10^{-10.6\pm1} \cdot \exp\left(-107 \pm 10\ \mathrm{kJ.mol^{-1}}/RT\right)$. These data have been compared with theoretical calculations from literature, showing reasonable agreement concerning the activation energy, but significant discrepancy regarding the D values.

Keywords: intermetallics (aluminides, silicides); diffusion; secondary ion mass spectrometry.

1. Introduction

Though the detrimental effect of oxygen as a contaminant on the mechanical properties of the TiAl alloys is recognized for a long time [1-5], the underlying mechanisms are still ignored. To address this issue, experimental measurements of oxygen diffusion coefficients in the γ and the α_2 phases is necessary to discriminate the hypotheses raised by these authors. Unfortunately, such data are lacking in the case of the TiAl intermetallics, even in the alloys currently employed in the industry. In particular, to interpret the striking phenomenon of embrittlement observed after short exposure durations (a few hours, typically) at low temperatures (down to 300°C) under air [5-14], experimental data on oxygen penetration kinetics are not available. Therefore, our objective in this study was to determine reliable experimental data of oxygen diffusion coefficient in the γ phase of TiAl. However, because the solubility of oxygen in the γ phase of TiAl is low (by atom probe tomography, values as low as 90 wt. ppm were reported [15]), its detection by conventional

microanalysis techniques is difficult. Moreover, even high-purity TiAl alloys are always contaminated by typically 500 wt ppm of oxygen [5], which creates additional detection difficulties.

Therefore, experiments were conducted in this study with the ^{18}O isotope of oxygen, to distinguish from the ^{16}O isotope constituting most of the oxygen contamination (the natural oxygen is constituted of 99.8 % of ^{16}O and 0.2 % of ^{18}O). Furthermore, the secondary ion mass spectrometry (SIMS) technique was selected, because of its high sensitivity to low solute concentrations and because of its ability to distinguish between isotopes. Note that this technique was already employed to successfully detect substantial decrease of oxygen content due to Nb alloying in binary $Ti_{45}Al_{55}$ and ternary $Ti_{44}Al_{52}Nb_4$ alloys, measurements in single crystalline $Ti_{45}Al_{55}$ alloys giving values of the order of 400 wt. ppm [16]. However, recent works have also proven the efficiency of the soft X-ray emission spectroscopy technique for measuring the oxygen content in the γ phase of TiAl alloys, by appropriately removing surface contamination layers using sputtering. Oxygen solubilities in γ-TiAl of the order of 800 wt. ppm for heat-treatments at 1100°C for 336 h have been obtained by this technique [17]. These values seem to be more reliable than those previously obtained by EPMA, which gave values of about 1-2 at. % [18] and of about 7 at. % [19], but without removing in these cases the surface contamination layers.

Theoretical oxygen diffusion coefficients in the γ phase of TiAl have been determined by three independent studies, which gave comparable results [20-23]. In these studies, the γ-TiAl L_{10} structure belonging to space group 123 (P4/mmm, tP2) was considered, in which the oxygen atoms occupy the stable 2h Wyckoff insertion position. Diffusion occurs by jumps between 2h and 2e insertion sites, and leads to different diffusion coefficient values in the (*x,y*) and (*z*) directions [20-23]. Surprisingly, quite elevated *D* values were predicted (*e.g.* 10^{-11} m^2/s at 700°C, meaning diffusion distances *d* of the order of 400 μm for 1 h of exposure, using for *d* the expression $d = 2\sqrt{Dt}$). An anisotropy of the diffusion coefficient values *D* has been predicted, the value perpendicular to the *z* = [001] crystalline axis being found to be about one order of magnitude higher than parallel to this direction. A slight anisotropy has also been found concerning the activation energies *Q*, values of 105-115 kJ/mol perpendicular to the [001] direction, and 115 kJ/mol parallel to [001], being calculated. However, strong interactions of the oxygen interstitials with antisites and substitutional solutes (like Nb and Cr for example) was predicted, which resulted in a decrease of the diffusion coefficient by 2-3 orders of magnitude [24]. One of the aims of our study is thus to compare these theoretical predictions with experimental results.

There are, however, scarce results of oxygen diffusion coefficient measurements in the phases of the Ti-Al system. In the α_2 phase, the data exhibit significant discrepancy. At 800° for example, values of $D = 4.6\text{-}6.2 \times 10^{-18}$ m^2/s [25] and $D = 1.1\times10^{-16}$ m^2/s [26] are reported. In this phase, one experimental activation energy is reported: Q =185 kJ/mol [25]. In γ-TiAl, no experimental diffusion data are reported. Measurements were carried out in amorphous layers of TiAl composition deposited by sputtering experiments, and values around 10^{-14} m^2/s at 700°C were obtained, with activation energies of about 175 kJ/mol [27]. This pioneering study gave thus interesting first experimental estimates of the oxygen diffusion coefficients in layers of

compositions close to that of γ-TiAl. However, it was not fully satisfactory, because the amorphous structure of the sputtered TiAl layer was suspected to induce pronounced thermal instability of the microstructure, which could significantly affect the oxygen diffusion kinetics.

Therefore, we have intended in the present work to experimentally measure the oxygen diffusion kinetics in the γ phase of a GE TiAl alloy. For this purpose, a model coarse-grained $Ti_{48.3}Al_{47.7}Cr_{1.9}Nb_{2.1}$ near-γ alloy was selected, which was exposed to Ar-1%$^{18}O_2$ at 500°C, 600°C and 700°C for different durations. Then, diffusion profiles have been obtained using the SIMS depth profiling technique.

2. Experimental

$Ti_{48.3}Al_{47.7}Cr_{1.9}Nb_{2.1}$ near-γ GE alloys were provided by SAFRAN Tech. Figure 1 shows that their microstructure was mainly composed of coarse grains of γ phase of about 100 µm in size, with some residual α_2 and B2 phases (≈ 2 vol. % in total). The initial oxygen content was measured by instrumental gas analysis by the EAG company (Toulouse, France), by heating the samples in graphite crucibles up to 2500°C, and by detecting oxygen emission as CO or CO_2 by infrared detectors. Initial oxygen contents were then between 400 wt. ppm and 500 wt. ppm depending on the samples. Square specimens 5×5×2 mm in size were cut by spark erosion, and polished down to 1 µm diamond suspension on all their faces to remove the surface contamination. These specimens were then heat-treated in a controlled atmosphere furnace. The chamber was first evacuated to 10^{-2} mbar before introducing the Ar-1%$^{18}O_2$ premix at a gas flow rate of a few ml/min, the $^{18}O_2$ gas of > 97% purity being supplied by the Eurisotop company. A bubbler filled with 2 cm of water ensured a slight overpressure in the furnace. Oxide films with interferometric colors were observed after heat treatments. The presence of submicronic oxide films on the surface of the samples assures us that the kinetics of oxygen penetration into the metal is controlled by the diffusion of oxygen into the metal, with the concentration of oxygen at the metal/oxide interface imposed by thermodynamic equilibrium.

Then, depth profiles of oxygen were obtained by secondary ion mass spectrometry (SIMS). The equipment used was a dynamic SIMS with magnetic sector (IMS7f from CAMECA). In order to obtain the best sensitivity for the detection of oxygen, the profiles were carried out with a primary Cs^+ ion beam of 10 keV. A negative voltage was applied between the sample and the extraction electrode (-5000 V) to extract negative ions. Under these conditions, the impact energy of the primary ions was of 15 keV, with an incidence angle of 27° with respect to the normal of the sample. The size of the scanned craters was 150×150 µm² and the primary current used was 40 nA. The analyzed area, limited by a diaphragm, had a diameter of 33 µm and was centered onto the scanned crater. The crater depths were measured following the analyzes using a stylus profiler (Dektak8 from BRUKER), which allowed to measure a sputtering rate of the TiAl matrix of 3.6 ± 0.5 µm/h. The analyzes were carried out under a vacuum of ~ 5.10^{-10} mbar. Therefore, considering the density of the primary ions used (J_p = 180 µA.cm^{-2}) that leads to a high sputtering rate, the influence of the residual vacuum on the results is negligible. The secondary ions recorded

for this study were $^{16}O^-$ and $^{18}O^-$ but also $^{1}H^-$, $^{12}C^-$ and $^{27}Al^-$. The intensity of the matrix element, $^{27}Al^-$, was around 1.2×10^5 cps for all profiles.

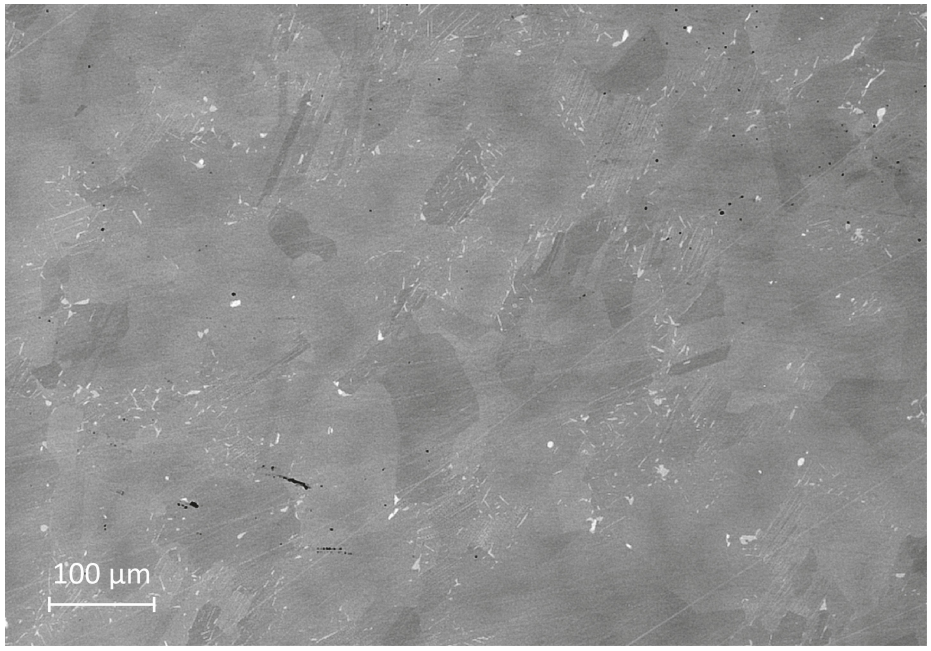

Fig. 1. Coarse-grained near-γ microstructure of the $Ti_{48.3}Al_{47.7}Cr_{1.9}Nb_{2.1}$ model alloy, showing γ phase in dark grey and residual α_2 and B2 phases as precipitates in light grey.

3. Results

Figure 2 shows ^{18}O depth profiles (SIMS intensities as a function of distance x from the metal-oxide interface), for exposure at 500°C, 600°C and 700°C in Ar-1%$^{18}O_2$ atmosphere. It can be seen that the ^{18}O signals exhibit marked maxima of $\approx 10^8$ cnt/s at the beginning of the profiles. This region can thus be associated to the thermally grown oxide scale that formed during exposure to the Ar-1%$^{18}O_2$ atmosphere. To define the position of the metal-oxide interfaces, we have used the inflexion points of the sharp drops of the ^{18}O signals after the $\approx 10^8$ cnt/s maxima, following the procedure described in Ref. [28]. This position, which can be estimated with ± 0.1 µm accuracy, defines therefore the origin of the diffusion profile ($x = 0$) of ^{18}O in the metallic γ-TiAl phase.

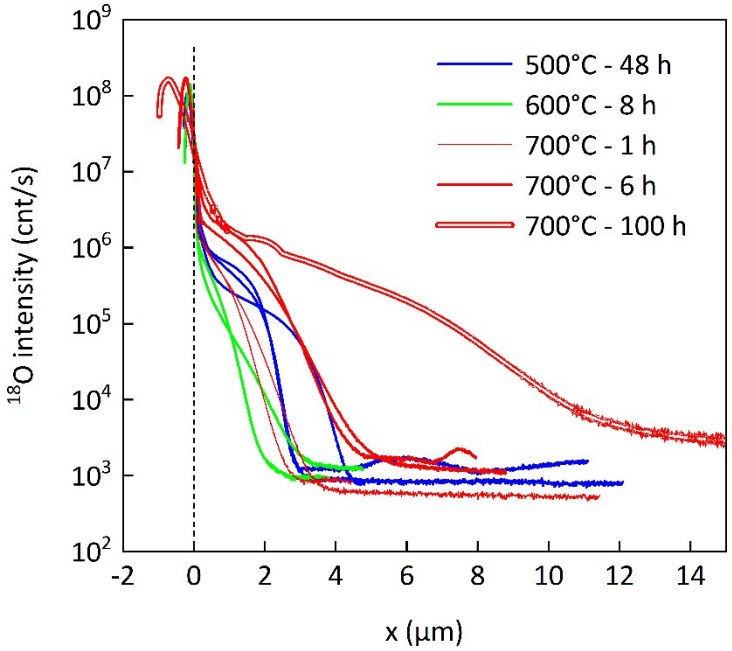

Fig. 2. ^{18}O depth profiles in γ-TiAl for various exposure conditions in Ar-1%$^{18}O_2$ atmosphere. The origin of the abscissa (x = 0 µm, indicated by a vertical dotted line) has been positioned at the inflexion points after the ≈ 10^8 cnt/s ^{18}O intensity maxima, that is, at the metal-oxide interface, according to the procedure described in Ref. [28].

Figure 3 shows separately, for the exposures at 500°C, 600°C and 700°C, the curves portions for which $x > 0$, to improve readability. During the diffusion experiments, the durations of the exposures have been adapted so that the diffusion profiles extend over comparable depths. Therefore, durations of 48 h, 8 h and 1 h have been selected for 500°C, 600°C and 700°C exposure temperatures, respectively. In each case, two profiles at least were acquired, to quantify the repeatability of the measurements. Moreover, additional exposures of 6 h and 100 h at 700°C have been carried out, to verify that similar diffusion coefficient values are derived whatever the exposure durations. Note that, in the cases of Figs. 3a and b, the profiles exhibit significant scattering in diffusion depths for given temperature and exposure durations (500°C-48 h for Fig. 3a, and 600°C-8 h for Fig. 3b). This will be interpreted in the Discussion section.

Using the profiles shown in Fig. 3, and making the assumption that the SIMS intensity I and the ^{18}O concentration are proportional to each other, the ^{18}O diffusion coefficient D in the γ-TiAl metallic phase have been deduced by adjusting the profiles by Erf functions in the form [29]:

$$c = c_0 + (c_s - c_0) \cdot \left(1 - \mathrm{Erf}\left[x \Big/ \left(2 \cdot \sqrt{Dt}\right)\right]\right) \qquad [2]$$

with $c \equiv I$, c_s: concentration in the γ-TiAl metallic phase at the metal-oxide interface, c_0: concentration at infinity, and t: time. For the adjustments, the whole dynamic of the detection range of the SIMS have been employed, taking advantage of the representation of the intensities in logarithmic scales. In all cases, the $^{18}O/^{16}O$ ratio in the diffusion profiles tended to the natural isotopic ratio ($^{18}O/^{16}O = 0.002$) far from the metal-oxide interface, which gave the upper limit of

the oxygen penetration depth. It can be seen that the profiles obtained at 700°C and 600°C can be accurately adjusted by the expression given by Equ. 2. However, the profiles obtained at 500°C could not be fitted over the entire intensity range. This will be discussed below. Nevertheless, thanks to the high dynamic of the SIMS measurements, the low intensity parts of the profiles could be used to carry out Erf fits in that case.

Note that the ^{18}O intensities were not converted into ^{18}O concentrations using the instrumental gas analyses (oxygen content in the $\gamma+\alpha_2$ alloy between 400 wt. ppm and 500 wt. ppm), because the very high oxygen content into the α_2 phase as compared to the γ phase (7000 wt. ppm and 90 wt. ppm, respectively, in a $Ti_{52}Al_{48}$ alloy [15]) would lead to strong overestimation of the oxygen content in the γ phase based on that of the $\gamma+\alpha_2$ alloy.

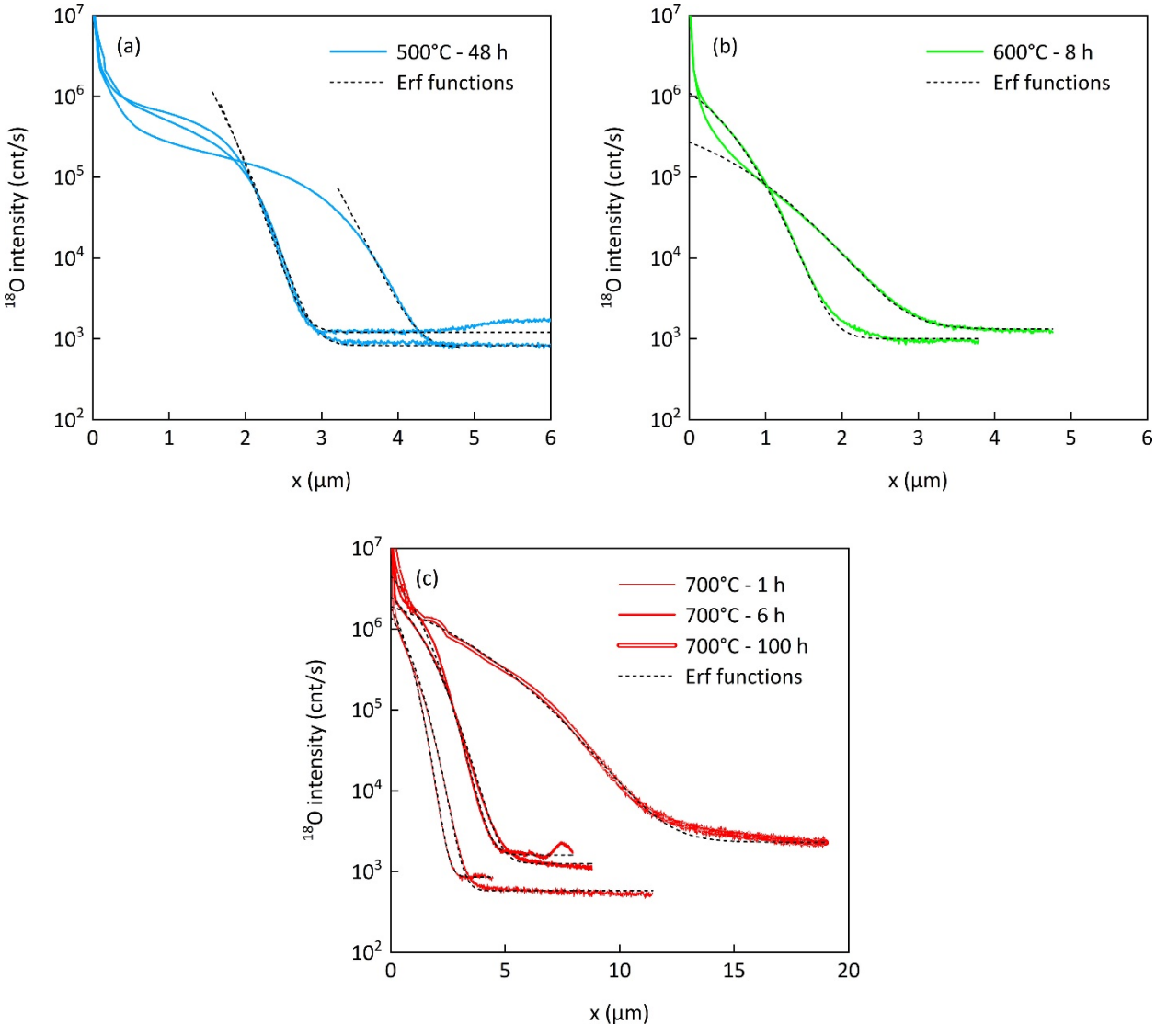

Fig. 3. ^{18}O depth profiles: intensity of the element as a function of distance from the metal-oxide interface x for different exposure temperature and duration conditions in Ar-1%^{18}O atmosphere. (a) 500°C. (b) 600°C. (c) 700°C.

Table 1 gives the diffusion coefficient data obtained by the Erf fits of the profiles using Equ. 2, and Fig. 4 shows these data plotted in the Arrhenius coordinates. From this graph, considering the spreading of the data, an activation energy of 107 ± 10 kJ/mol can be calculated. Thus, the expression to calculate the oxygen diffusion coefficient D in the γ phase of the $Ti_{48.3}Al_{47.7}Cr_{1.9}Nb_{2.1}$ alloy is as follows:

$$D\left(\mathrm{m^2/s}\right) = 10^{-10.6\pm1}\cdot\exp\left(\frac{-107\pm10\ \mathrm{kJ/mol}}{RT}\right) \quad [3]$$

Table 1. Obtained ^{18}O diffusion coefficient data.

Sample #	Exposure conditions : Temperature – Time	^{18}O diffusion coefficient (m^2/s)
1	500°C – 48 h	2.5×10^{-18}
2	500°C – 48 h	1.2×10^{-18}
3	500°C – 48 h	1.1×10^{-18}
4	600°C – 8 h	1.6×10^{-17}
5	600°C – 8 h	5.3×10^{-18}
6	700°C – 1 h	1.1×10^{-16}
7	700°C – 1 h	7.1×10^{-17}
8	700°C – 6 h	4.2×10^{-17}
9	700°C – 6 h	3.3×10^{-17}
10	700°C – 100 h	1.8×10^{-17}

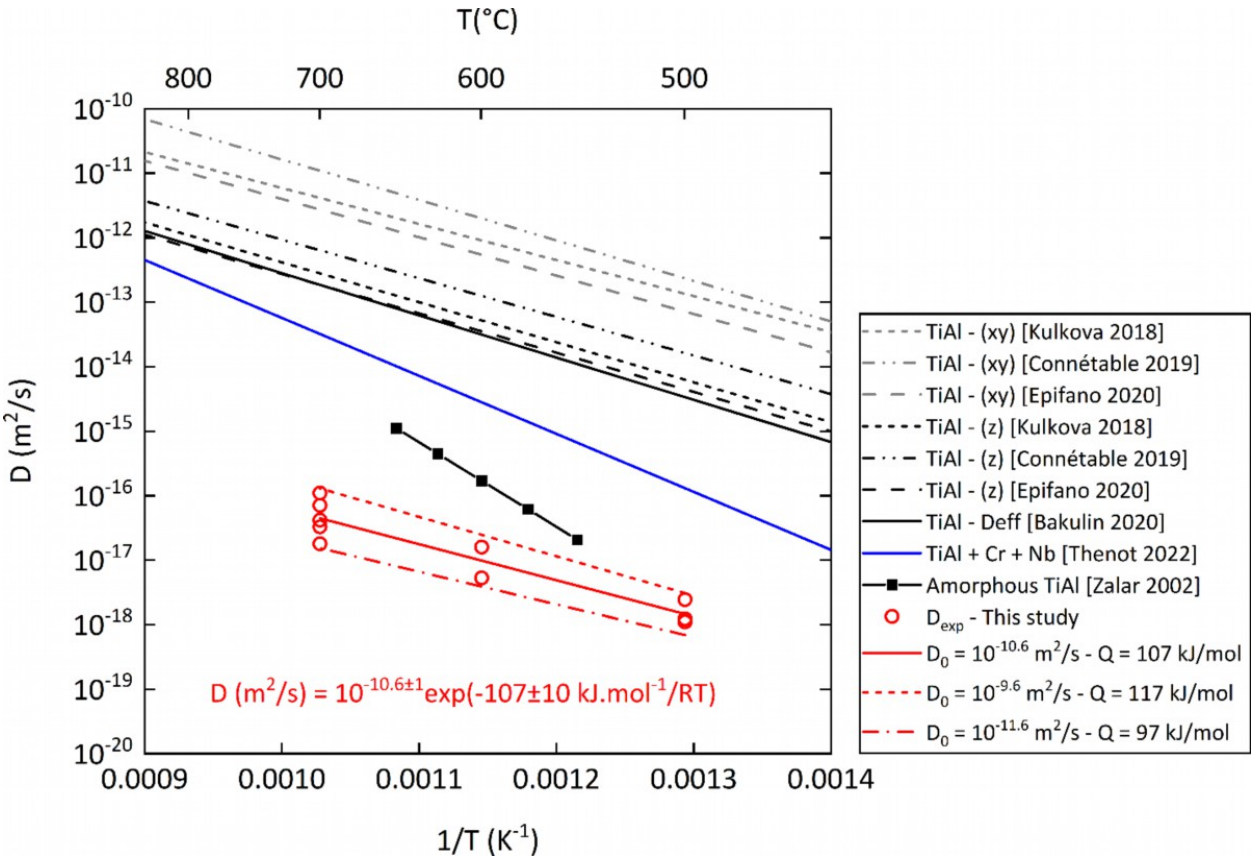

Fig. 4. Experimental ^{18}O diffusion coefficients in γ-$Ti_{48.3}Al_{47.7}Cr_{1.9}Nb_{2.1}$ obtained in this study (red symbols, with red lines giving indicative $D = D_0 \exp(-Q/RT)$ expressions reflecting the scattering of the data), compared with literature theoretical and experimental data (TiAl-(xy) and TiAl-(z) meaning theoretical diffusion coefficient values in the (xy) plane and along the z direction of the tetragonal crystalline cell of TiAl, respectively). [Kulkova 2018] = [20], [Connétable 2019] = [21], [Epifano 2020] = [23], [Bakulin 2020] = [22], [Thenot 2022] = [24], [Zalar 2002] = [27].

4. Discussion

Figure 5 shows an example of ^{18}O and ^{16}O intensity profiles ($I^{18}O$ and $I^{16}O$), and of the $I^{18}O/(I^{16}O+I^{18}O)$ profile, as a function of diffusion distance x from the metal/oxide interface. It can be seen that the $I^{18}O/(I^{16}O+I^{18}O)$ ratio, which is usually considered for studying diffusion of oxygen, exhibits a constant value close to the origin ($x = 0$). This kind of behavior is hardly compatible with usual diffusion profiles, for which the slope close to $x = 0$ is maximum most of the time. Moreover, the $I^{16}O$ signal (red dotted line) exhibits a shape resembling that of a regular diffusion profile close to $x = 0$. Therefore, we think that this can be interpreted by the penetration of $I^{16}O$ coming from various origins, like the contamination of the $^{18}O_2$ and/or Ar gas, or the presence of leaks in the furnace allowing air to contaminate the Ar-1% $^{18}O_2$ mixture, or the diffusion of oxygen adsorbed on the sample surface during the exposure at high temperature. Therefore, close to the metal-oxide interface ($x = 0$), both ^{18}O and ^{16}O diffuse at the same speed,

and the corresponding $I^{18}O$ and $I^{16}O$ exhibit thus the same shape. Therefore, the $I^{18}O/(I^{16}O+I^{18}O)$ ratio is consequently constant. But, when the diffusion depth increases, the $I^{16}O$ signal tends to a value corresponding to the signal coming from the contamination by ^{16}O in the alloy prior to exposure at high temperature to Ar-1% $^{18}O_2$, whereas the $I^{18}O$ signal tends to a much lower value, corresponding the $^{18}O/^{16}O$ natural isotopic ratio (=0.002) in the oxygen initially contaminating the alloy. Therefore, the $I^{18}O/(I^{16}O+I^{18}O)$ ratio continuously decreases, down to the natural isotopic ratio. Because the corresponding profile is more complex to interpret in terms of diffusion coefficient than that of the $I^{18}O$ signal, we selected the latter for the calculation of the diffusion coefficients. Moreover, it can be seen that, from $x \approx 2$ µm and above, the ^{16}O signal is almost constant, and corresponds thus to the ^{16}O initially present in the alloy as a contaminant. Because this signal is constant, there is no need to compensate for matrix effects using the $I^{18}O/(I^{16}O+I^{18}O)$ ratio. Finally, because the external sources of ^{16}O were not controlled (contamination of the atmosphere and/or of the sample surfaces), we chose to not consider the ^{16}O profiles for calculating the diffusion profiles.

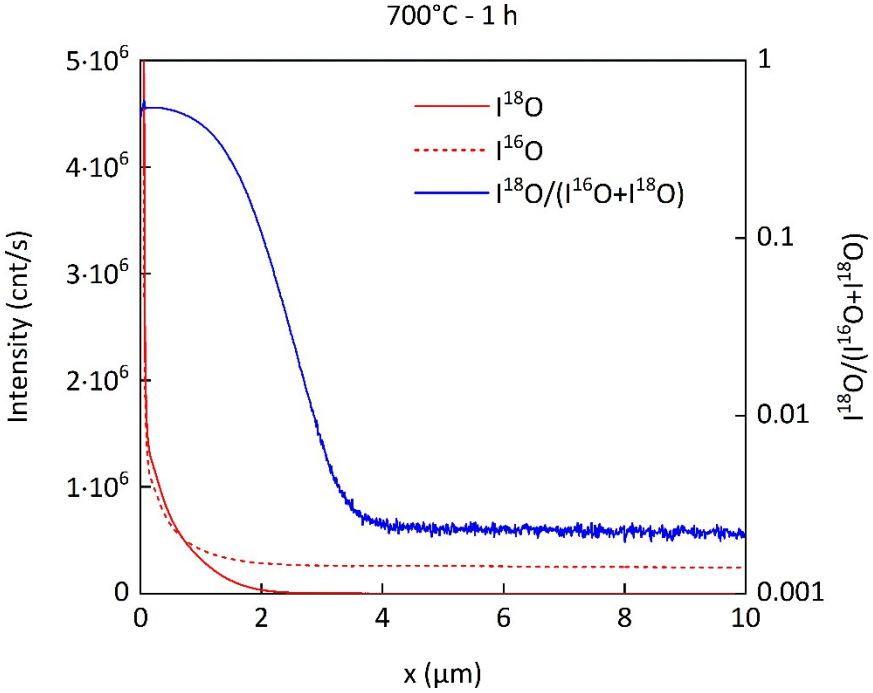

Figure 5. Intensities I of the ^{18}O and ^{16}O signals, and $I^{18}O/(I^{16}O+I^{18}O)$ ratio, as a function of diffusion distance x from the metal/oxide interface, in the case of a sample exposed at 700°C for 1 h in Ar-1%$^{18}O_2$ atmosphere.

Figure 3 shows that, for the heat treatments at 600°C and 700°C, the concentration profiles can be quite accurately adjusted by the expression in Erf function given by Equ. 2, particularly on two decades in the low ^{18}O concentration range. Therefore, we believe that, in these cases, our results give first reliable experimental estimates of the oxygen diffusion kinetics in the γ phase of TiAl. However, for the profiles obtained at 600°C, if the shapes of the two profiles correspond well to Erf functions, they do not superimpose to each other, and the penetration depths are significantly different: about 2-3 µm for one profile, and about 3-4 µm for the other. The analysis

of these profiles leads to diffusion coefficient values of 5.3×10^{-18} m^2/s and 1.6×10^{-17} m^2/s, respectively. Moreover, from the profiles obtained at 700°C, diffusion coefficient data ranging from 1.8×10^{-17} m^2/s and 1.1×10^{-16} m^2/s are obtained. Therefore, the typical scattering of our data is of about one order of magnitude. However, the theoretical predictions from literature presented in Fig. 4 show that the diffusion coefficient values can exhibit significant differences depending on the diffusion direction in the tetragonal crystalline cell of TiAl [20, 21, 23]. In particular, diffusion in the *(xy)* plane is predicted to be about one order of magnitude faster than along the *z* direction. Therefore, the observed scattering in our experimental data is attributed to this effect.

The shape of the profiles obtained at 500°C, which deviate significantly from Erf functions in the high concentration ranges, is less understood. One potential interpretation is that the regions investigated on the corresponding samples contained a higher fraction of α_2 and/or B2 phases than the samples exposed at 600°C and 700°C. Therefore, if α_2 or B2 precipitates are included in the sputtered volume during the SIMS acquisitions, the higher oxygen content of these phases can largely modify the shape of the concentration profiles. Unfortunately, the surface roughness of the bottom of the SIMS craters prevented the verification of this hypothesis. But if this hypothesis is correct, after the whole α_2 or B2 precipitate has been sputtered, the diffusion profile in the low concentration regime is again representative of diffusion of ^{18}O in the γ phase. This is why the profiles, in these cases, have been adjusted by Erf functions taking only into account the low concentration range.

Moreover, Table 2 gives a comparison of the activation energy determined in our study with theoretical calculations [20-24], and with few other experimental data available [25-27]. It can be noticed that the value obtained in our study, 107 ± 10 kJ/mol, is close to theoretical values obtained in binary TiAl considering an interstitial mechanism, 105-115 kJ/mol [20-23], but is lower than that obtained in the case of quaternary TiAl + Cr + Nb, 172 kJ/mol [24]. This suggests that the calculations of the activation energy of the interstitial mechanism captures quite realistically the actual physical diffusion process, but that the influence of solutes like Cr and Nb tends to be overestimated by the calculations. The activation energy obtained in our study is also lower than that obtained experimentally in amorphous layers of TiAl composition [27], which is surprising, because amorphous materials are believed to exhibit higher free volume, which would lower the activation barriers for the atomic jumps. However, the effect of the lower free volume of the amorphous Ti-Al layers on the absolute values of the diffusivities would, on the contrary, lead to higher kinetics than in crystalline TiAl γ grains, which is the case here.

Table 2. Summary of literature results of oxygen diffusion in γ-TiAl. (xy) and (z) refers to diffusion in the x = [100], y =[010] and z = [001] directions of the crystalline cell, respectively.

Matrix	Method of determination	Activation energy (kJ/mol)	Ref.
γ-TiAl	DFT	(*xy*): 107 (*z*): 118	[20]
γ-TiAl	DFT	(*xy*): 120 (*z*): 115	[21]
γ-TiAl	DFT	125	[22]
γ-TiAl	DFT	114	[23]
γ-TiAl	DFT Calculations taking into account Cr and Nb substitutional solutes	172	[24]
50Ti-50Al	Amorphous sputtered layer of 50Ti-50Al (at. %) composition, Auger spectroscopy	175	[27]
γ-TiAl	Coarse-grained near γ $Ti_{48.3}Al_{47.7}Cr_{1.9}Nb_{2.1}$, SIMS	107 ± 10	This study
α_2-Ti_3Al	α_2-Ti_3Al single crystal grown by floating zone, O_2^+ ion implantation, Auger sputter depth profiling	185	[25]

Considering now the experimental diffusion coefficient data of this study compared with theoretical data from literature [20-23], differences of 2 to 3 orders of magnitude are observed, which is significant. This discrepancy remains also when the effect of trapping of oxygen by point defects (antisites) and solutes is taken into account [24], an even greater slowdown than predicted being observed. One potential explanation to account for this discrepancy could result from an insufficient accuracy, in the theoretical calculations, in the determination of the pre-exponential factor D_0 in the usual expression of the diffusion coefficient: $D = D_0 \cdot \exp(-Q/RT)$. In particular, the jump-attempt frequencies [21] need probably to be estimated with greater precision. This shows that the oxygen diffusion mechanism in an intermetallic system like TiAl, in spite of its apparent simplicity, remains complex. In particular, the approximations in the atomic scale

mechanisms which have been neglected in the theoretical predictions, deserve now deeper analyzes.

5. Conclusions

In this study, reliable data of oxygen diffusion kinetics in the γ phase of a $Ti_{48.3}Al_{47.7}Cr_{1.9}Nb_{2.1}$ alloy have been obtained, by implementation of a methodology based on diffusion experiments of ^{18}O isotopes and on SIMS depth profiling. From these measurements, the following expression has been derived for oxygen diffusion: $D\left(\mathrm{m^2/s}\right) = 10^{-10.6\pm1}\cdot\exp\left(-107 \pm 10\ \mathrm{kJ.mol^{-1}}/RT\right)$. The obtained activation energy Q is compatible with theoretical calculations of diffusion by an interstitial mechanism, even if the experimental D values are significantly lower than those predicted.

Acknowledgments

The authors wish to warmly thank F. Jomard from the GEMaC laboratory (Versailles) for fruitful discussions. This project was funded by the French Agence Nationale de la Recherche project DEMENTIAL, grant ANR-21-CE08-0040. This work was supported by the Région Occitanie, France, grant ALDOCT-000691/19008725, and Safran Tech, France, which are also acknowledged.

References

[1] T. Takasugi, S. Hanada, M. Yoshida, Environmental embrittlement of γ titanium aluminide, J. Mater. Res. 7 (1992) 2736-2746.

[2] T. Kawabata, T. Abumiya, O. Izumi, Effect of oxygen addition on mechanical properties of TiAl at 293–1273 K, Acta Metallurgica et Materialia, 40 (1992) 2557-2567.

[3] Y.G. Nakagawa, K. Matsuda, S. Masaki, R. Imamura, M. Arai, Gamma titanium aluminides (Y.W. Kim , R. Wagner , M. Yamaguchi eds), TMS, Warrendale, PA, 1995, p. 415.

[4] M. Lamirand, J. Bonnentien, G. Ferrière, S. Guérin, J. Chevalier, Effects of interstitial oxygen on microstructure and mechanical properties of Ti-48Al-2Cr-2Nb with fully lamellar and duplex microstructures, Metall. Mater. Trans. A 37A (2006) 2369-2378.

[5] F. Appel, J. Paul, M. Oehring, Gamma Titanium Aluminide Alloys, Wiley, Weinheim, 2011.

[6] W. Dowling, W. Donlon, The effect of surface film formation from thermal exposure on the ductility of Ti-48Al-1V-0.2C, Scr. Metall. Mater. 27 (1992) 1663.

[7] C. Austin, T. Kelly, Structural Intermetallics, TMS, Warrendale, 1993.

[8] T. Kelly, C. Austin, P. Fink, J. Schaeffer, Effect of elevated temperature exposure on cast gamma titanium aluminide (Ti-48Al-2Cr-2Nb), Scr. Metall. Mater. 30 (1994) 1105.

[9] D.S. Lee, M.A. Stucke, D.M. Dimiduk, Effects of thermal exposure on the properties of two γ alloys, Mater. Sci. Eng. A192 (1995) 824-829.

[10] A. Planck, S. Rosenberger, Gamma titanium aluminides, TMS, Warrendale, 1999.

[11] S. Draper, B. Lerch, I. Locci, M. Shazly, V. Prakash, Effect of exposure on the mechanical properties of gamma met PX, Intermetallics 13 (2005) 1014-1019.

[12] M. Thomas, O. Berteaux, F. Popoff, M. Bacos, A. Morel, B. Passilly, V. Ji, Effects of exposure at 700°C on RT tensile properties in a PM γ-TiAl alloy, Intermetallics 14 (2006) 1143.

[13] X. Wu, A. Huang, D. Hu, M.H. Loretto, Oxidation-induced embrittlement of TiAl alloys, Intermetallics 17 (2009) 540-552.

[14] P. Sallot, J. Monchoux, S. Joulié, A. Couret, M. Thomas, Impact of β-phase in TiAl alloys on mechanical properties after high temperature air exposure, Intermetallics 119 (2020) 106729.

[15] A. Denquin, S. Naka, A. Huguet, A. Menand, Atom-probe investigation of the partitioning of interstitial elements in two-phase γ + α2 TiAl-based alloys, Scr. Metall. Mater. 28 (1993) 1131-1136.

[16] S. Oswald, R. Hermann, B. Schmidt, SIMS measurement of oxygen content in γ-TiAl single crystals and polycrystalline alloys with Nb addition, Materials Science and Engineering A 516 (2009) 54-57.

[17] H. Nakashima, A. Kinouchi, M. Takeyama, Quantitative analysis of oxygen in solution in the Ti-Al-O ternary alloys by soft X-ray emission spectroscopy, Journal of Alloys and Compounds 920 (2022) 165822.

[18] M.X. Zhang, K.C. Hsieh, J. DeKock, Y.A. Chang, Phase diagram of Ti-Al-O at 1100°C, Scr. Metall. Mater. 27 (1992) 1361–1366.

[19] V. Shemet, P. Karduck, H. Hoven, B. Grushko, W. Fischerd, W.J. Quadakkers, Synthesis of the cubic Z-phase in the Ti-Al-O system by a powder metallurgical method, Intermetallics 5 (1997) 271–280.

[20] S. Kulkova, A. Bakulin, S. Kulkov, First-principles calculations of oxygen diffusion in Ti-Al alloys, Latv. J. Phys. Tech. Sci. 55 (2018) 20–29.

[21] D. Connétable, A. Prillieux, C. Thenot, J.P. Monchoux, Theoretical study of oxygen insertion and diffusivity in the γ-TiAl L_{10} system, Journal of Physics: Condensed Matter 32 (2020) 175702.

[22] A.V. Bakulin, S. Kulkov, S. Kulkova, Diffusion properties of oxygen in the γ-TiAl alloy, J. Exp. Theor. Phys. 130 (2020) 579-590.

[23] E. Epifano, G. Hug, First-principle study of the solubility and diffusion of oxygen and boron in γ-TiAl, Comput. Mater. Sci. 174 (2020) 109475.

[24] C. Thenot, R. Besson, P. Sallot, J.P. Monchoux, D. Connétable, Interactions of oxygen with intrinsic defects in $L1_0$ γ-TiAl in presence of substitutional solutes: influence on diffusion kinetics, Computational Materials Science 201 (2022) 110933.

[25] Y. Koizumi, M. Kishimoto, Y. Minamino, H. Nakajima, Oxygen diffusion in Ti_3Al single crystals, Phil. Mag. 88 (2008) 2991–3010.

[26] S. Draper, D. Isheim, Environmental embrittlement of a third generation γ TiAl alloy, Intermetallics 22 (2012) 77–83.

[27] A. Zalar, J. van Lier, E.J. Mittemeijer, J. Kovac, Interdiffusion at TiO_2/Ti TiO_2/Ti_3Al and TiO_2/TiAl interfaces studied in bilayer structures, Surf. Interface Anal. 34 (2002) 514–518.

[28] O. Gebhardt, SIMS depth profiling, line scanning and imaging analyses of the oxide layer on in-reactor corroded cladding specimens with high lateral resolution, Fresenius J. Anal. Chem. 365 (1999) 117-122.

[29] Y. Adda, J. Philibert, La diffusion dans les solides, Institut national des sciences et techniques nucléaires, Saclay, 1966.